

Article

CA₄Mg^{0/−}: Global Minima with a Planar Tetracoordinate Carbon Atom

Nisha Job¹, Maya Khatun², Krishnan Thirumoorthy¹, Sasanka Sankhar Reddy CH³,
Vijayanand Chandrasekaran¹, Anakuthil Anoop^{2,*} and Venkatesan S. Thimmakondur^{4,*}

¹ Department of Chemistry, School of Advanced Sciences, Vellore Institute of Technology, Vellore 632 014, Tamil Nadu, India; nisha.job2019@vitstudent.ac.in (N.J.); thirumoorthy.krishnan@vit.ac.in (K.T.); vijayanand.c@vit.ac.in (V.C.)

² Department of Chemistry, Indian Institute of Technology Kharagpur, Kharagpur 721 302, West Bengal, India; mayakhatun@iitkgp.ac.in

³ Department of Electrical and Electronics Engineering, Birla Institute of Technology and Science, Pilani-K K Birla Goa Campus, Goa 403 726, India; sankharreddy@outlook.com

⁴ Department of Chemistry and Biochemistry, San Diego State University, San Diego, CA 92182-1030, USA

* Correspondence: anoop@chem.iitkgp.ac.in (A.A.); vthimmakondusamy@sdsu.edu (V.S.T.)

Abstract: Isomers of CA₄Mg and CA₄Mg[−] have been theoretically characterized for the first time. The most stable isomer for both the neutral and anion contain a planar tetracoordinate carbon (ptC) atom. Unlike the isoivalent CA₄Be case, which contains a planar pentacoordinate carbon atom as the global minimum geometry, replacing beryllium with magnesium makes the ptC isomer the global minimum due to increased ionic radii of magnesium. However, it is relatively easier to conduct experimental studies for CA₄Mg^{0/−} as beryllium is toxic. While the neutral molecule containing the ptC atom follows the 18 valence electron rule, the anion breaks the rule with 19 valence electrons. The electron affinity of CA₄Mg is in the range of 1.96–2.05 eV. Both the global minima exhibit π/σ double aromaticity. Ab initio molecular dynamics simulations were carried out for both the global minima at 298 K for 10 ps to confirm their kinetic stability.

Keywords: CA₄Mg; CA₄Mg[−]; planar tetracoordinate carbon; π/σ double aromaticity; global minima; anti-van't Hoff Le Bel



Citation: Job, N.; Khatun, M.; Thirumoorthy, K.; CH, S.S.R.; Chandrasekaran, V.; Anoop, A.; Thimmakondur, V.S. CA₄Mg^{0/−}: Global Minima with a Planar Tetracoordinate Carbon Atom. *Atoms* **2021**, *9*, 24. <https://doi.org/10.3390/atoms9020024>

Academic Editor: Kirill Tuchin

Received: 16 March 2021

Accepted: 7 April 2021

Published: 9 April 2021

Publisher's Note: MDPI stays neutral with regard to jurisdictional claims in published maps and institutional affiliations.



Copyright: © 2021 by the authors. Licensee MDPI, Basel, Switzerland. This article is an open access article distributed under the terms and conditions of the Creative Commons Attribution (CC BY) license (<https://creativecommons.org/licenses/by/4.0/>).

1. Introduction

The concept of planar tetracoordinate carbon (ptC) or carbon group elements enthralls both experimentalists [1–10] and theoreticians [11–19] as it is a fundamental deviation from the conventional ideas of tetrahedral tetracoordinate carbon [20,21]. The latter was defined independently by van't Hoff and Le Bel in 1874. In 1968, Monkhorst first mentioned the idea of ptC as a transition state geometry in a non-dissociative racemization process [22]. In 1970, Hoffmann and co-workers showed ways to stabilize ptC by incorporating appropriate substituents that would act as a good σ -donor/ π -acceptor simultaneously or by embedding the ptC into a $(4n + 2)\pi$ electron system [11]. In 1976, Schleyer and co-workers computationally identified, for the first time, the real minima (local, not global) in lithium substituted cyclopropane and cyclopropene [12]. Since then, many molecules containing ptC have been characterized in silico [23–32], and some have been experimentally detected [1–9]. Lately, the idea of ptC has been extended to planar hypercoordinate carbon (phC; penta [33–35] and hexa [36–40] coordination) as well as to other elements such as B [41,42] or N [43] considering their potential applications in material science [44,45].

Perhaps, making molecules containing ptC atoms remains an open challenge to date, although limited amount of success persists experimentally. While the thermodynamic and kinetic stability of these molecules have been greatly emphasized over the years [46,47], the less spoken issue in this endeavor for the purpose of experimental viability is the combination of atoms in achieving the ptC. In the past, many ptC or phC molecules containing

beryllium as one constituent elements have been proposed [28,30,39,48]. However, none of them have been experimentally achieved despite their experimental viability. One of the major safety issues in using beryllium is that it can cause the development of chronic beryllium disease [49]. For this reason, beryllium chemistry is somewhat underdeveloped from an experimental perspective [50]. Thus, we aimed to theoretically achieve ptC/phC without using beryllium. Here, the potential energy surfaces (PESs) of $\text{CAI}_4\text{Mg}^{0/-}$ have been characterized computationally using density functional theory and coupled-cluster methods. The global minimum geometries of both the neutral and anion contain a ptC atom (see Figure 1). The isovalent system of the neutral, CAI_4Be , has been explored elsewhere [30], where the global minimum geometry contains a planar pentacoordinate carbon (ppC). By replacing beryllium with magnesium, one could achieve ptC instead of ppC due to the increased ionic radius of magnesium.

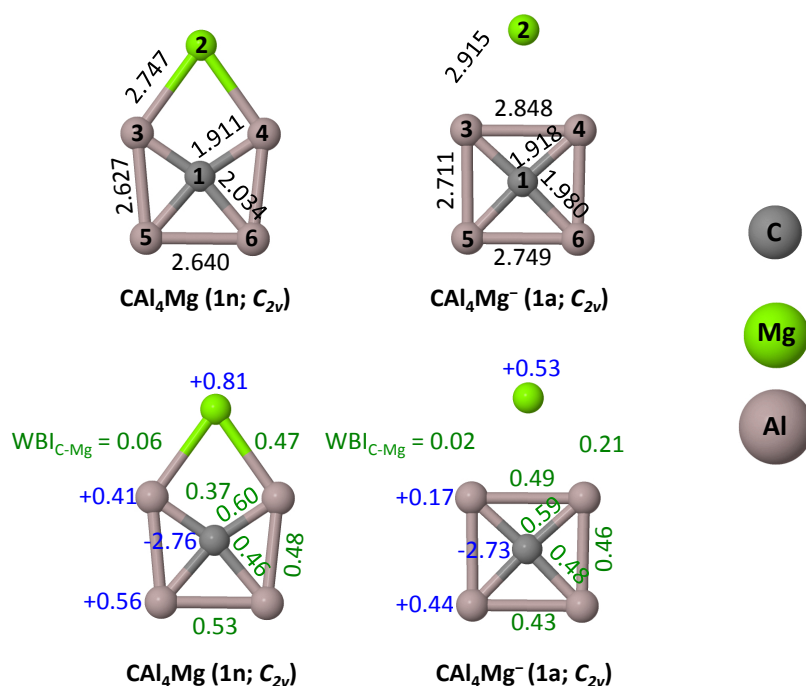


Figure 1. Global minimum structures of CAI_4Mg (1n) and CAI_4Mg^- (1a). Bond lengths are given in Å in the top row. The atom numbering scheme used herein is also shown. Natural atomic charges (in $|e|$; blue color) and Wiberg bond indices (green color) calculated at the $(U)\omega\text{B97XD}/6\text{-311++G}(2\text{d},2\text{p})$ level are given in the bottom row.

2. Computational Details

Several trial geometries of CAI_4Mg and CAI_4Mg^- are generated by chemical intuition and the cluster building procedure implemented in PyAR [51,52]. Modeling by intuition was done targeting for ptC and phC based on similar reported molecules. The automated cluster building is done as follows: First, a diatomic molecule is generated from two randomly chosen atoms from C, Al and Mg. To the optimized geometry of these diatomic molecules, another randomly chosen atom is added following the procedure described by Khatun et al. [52] to generate several (N) guess geometries. All these geometries are optimized and unique minima are chosen and further addition of random atoms are continued until the target chemical formula is reached. We performed nine different runs with $N = 16$ orientations for both the neutral and anionic systems. The trial geometries were optimized using the ORCA program [53] interfaced with PyAR [51,52]. The initial geometry optimizations were carried out using PBE [54] functional with def2-SVP [55] basis set including Grimme's empirical dispersion corrections (D3) [56] with Becke–Johnson (BJ) damping [57,58] and resolution of the identity (RI) approximation. After we filtered all

geometries generated from nine different runs, unique geometries were selected for further analysis. Some geometries were reached from both intuitive and stochastic procedures. Overall, for CAI_4Mg and CAI_4Mg^- , we identified 37 and 33 stationary points, respectively.

The geometries of all $\text{CAI}_4\text{Mg}^{0/-}$ isomers reported here were optimized further using DFT with the (U) ω B97XD hybrid functional [59] and the 6-311++G(2d,2p) basis set [60,61]. Harmonic vibrational frequencies were calculated for each stationary point to confirm whether it is a minimum, transition state, or higher-order saddle-point. The number of imaginary frequencies (NImag) obtained for each stationary point are indicated underneath the geometries (see Figures 2 and 3). To obtain accurate relative energies, calculations were also done using the composite method, CBS-QB3 [62], for all the low-lying isomers lying within $23.06 \text{ kcal mol}^{-1}$ (1 eV). Wavefunction stability analysis was done for both the global minima (**1n** and **1a**) obtained at the (U) ω B97XD/6-311++G(2d,2p) level and no instabilities were found [63].

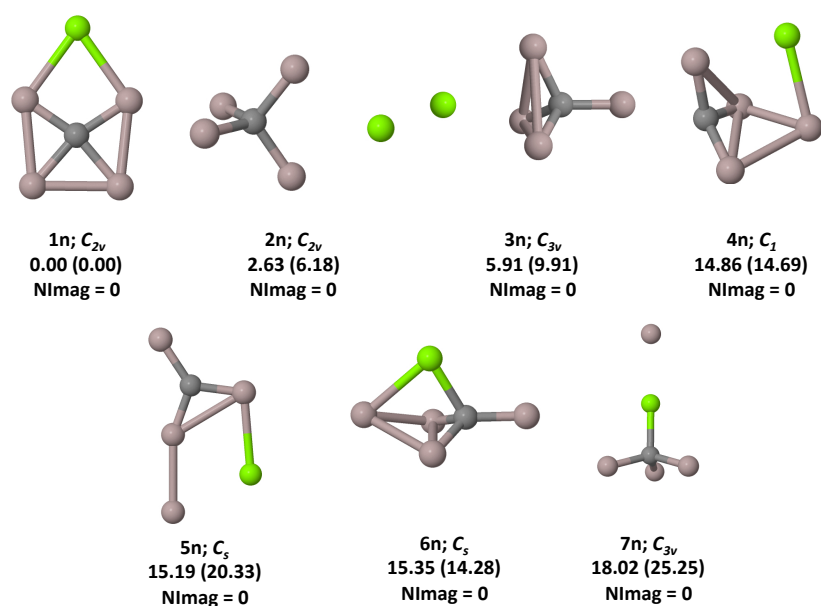


Figure 2. Low-lying isomers of CAI_4Mg on the singlet PES. Relative energies including ZPVE correction (in kcal mol^{-1}) are calculated at the ω B97XD/6-311++G(2d,2p) level. Relative energies obtained at the CBS-QB3 level are shown in parentheses. Number of imaginary frequencies (NImag) obtained for each stationary point are indicated underneath the geometries.

Nucleus independent chemical shift (NICS) [64] values were calculated to gauge the π/σ dual aromaticity in both the global minima. Chemical bonding in the global minima was analyzed using canonical molecular orbitals (CMOs), adaptive natural density partitioning (AdNDP) [65,66], and natural bond order (NBO) approach [67]. Natural atomic charges (q) and Wiberg bond indices (WBIs) [68] from the NBO analyses were calculated at the (U) ω B97XD/6-311++G(2d,2p) level. To assess the multi-reference character of each molecule, as suggested elsewhere [69], T_1 diagnostic value was calculated. All these calculations were carried out with the Gaussian suite of programs [70].

Topological analysis of electron localization function (ELF) and Laplacian of electron density were carried out for both the neutral and anionic global minima with Multiwfn program [71] using the wave function file generated by Gaussian program [70]. We performed ab initio molecular dynamics (AIMD) simulations using the atom-centered density matrix propagation (ADMP) [72] approach included in Gaussian 16 program [70] for the global minimum structures of CAI_4Mg and CAI_4Mg^- to check the kinetic stability of these molecules. These simulations were done for 10 ps at 298 K.

For brevity, optimized geometries of high-energy isomers, Cartesian coordinates of all isomers, total energies, zero-point vibrational energies (ZPVEs), net dipole moment and relative energies without and with ZPVE correction are given in the Supplementary Materials.

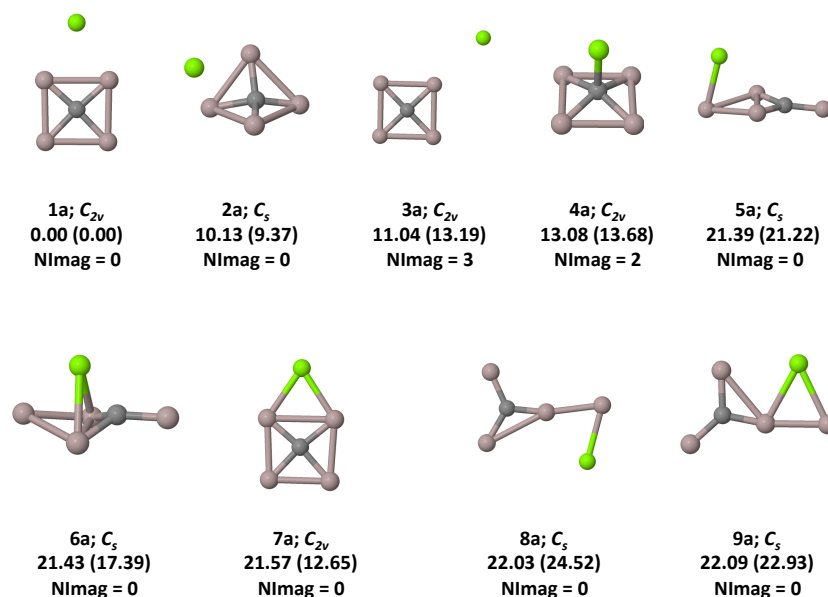


Figure 3. Low-lying isomers of CAI_4Mg^- on the doublet PES. Relative energies including ZPVE correction (in kcal mol^{-1}) are calculated at the $U\omega B97XD/6-311++G(2d,2p)$ level. Relative energies obtained at the CBS-QB3 level are shown in parentheses. The number of imaginary frequencies (NImag) obtained for each stationary point are indicated underneath the geometries.

3. Results and Discussion

The optimized geometries of the global minimum structures of CAI_4Mg (**1n**) and CAI_4Mg^- (**1a**) are shown in the top row of Figure 1. Natural atomic charges (q) and Wiberg bond indices are shown in the bottom row of Figure 1. The low-lying isomers of CAI_4Mg and CAI_4Mg^- are shown in Figures 2 and 3, respectively. ZPVE-corrected relative energies obtained at the $\omega B97XD/6-311++G(2d,2p)$ (for neutrals) and $U\omega B97XD/6-311++G(2d,2p)$ (for anions) levels are given for each geometry. The same obtained at the CBS-QB3 level are given in parentheses. Canonical molecular orbitals are shown in Figure 4. The bonding pattern obtained from AdNDP analyses is shown in Figure 5. NICS values calculated at 0 and 1 Å (NICS (0) and NICS (1)) are shown in Figure 6. Color filled map of ELF for **1n** and **1a** are shown in Figure 7. Gradient lines map of Laplacian of Electron Density ($\nabla^2\rho(r)$) with bond paths for **1n** and **1a** are shown in Figure 8. Bond length evolution of **1n** and **1a** obtained through ab initio MD simulations at 298 K in 10 ps are shown in Figure 9. Energy evolution of **1n** and **1a** calculated through ab initio MD simulations are shown in Figures 10 and 11, respectively.

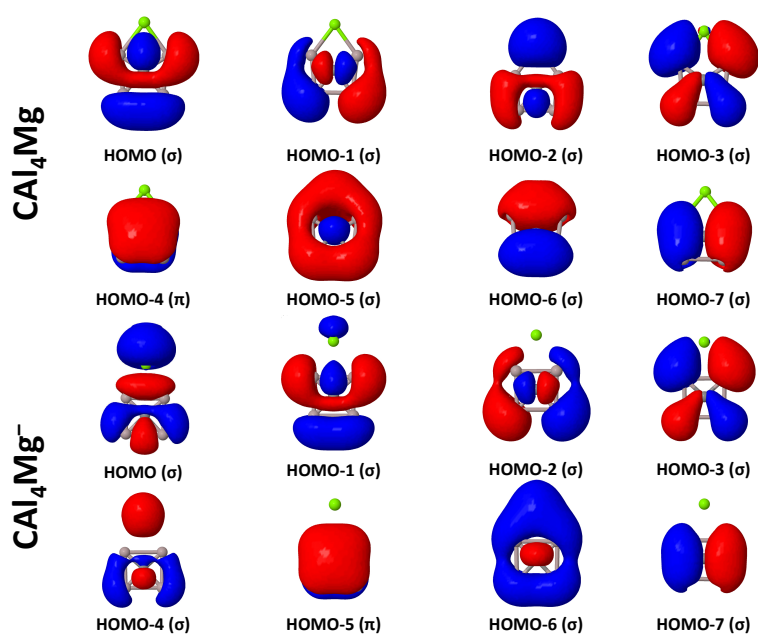


Figure 4. Canonical molecular orbitals (CMOs) of CAI_4Mg (**1n**) and CAI_4Mg^- (**1a**) obtained at the $(\text{U})\omega\text{B97XD}/6\text{-311++G}(2\text{d},2\text{p})$ level.

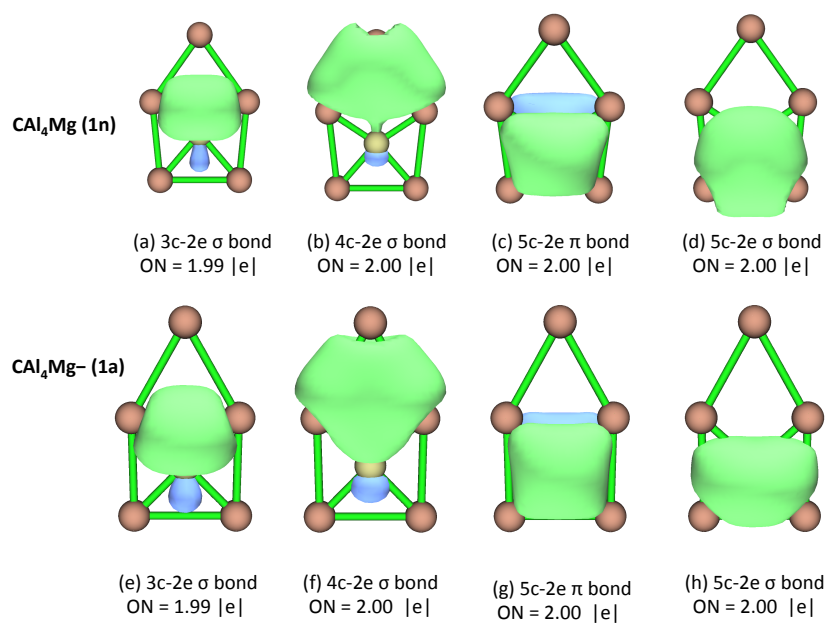


Figure 5. AdNDP bonding patterns of CAI_4Mg (**1n**) and CAI_4Mg^- (**1a**) obtained at the $(\text{U})\omega\text{B97XD}/6\text{-311++G}(2\text{d},2\text{p})$ level.

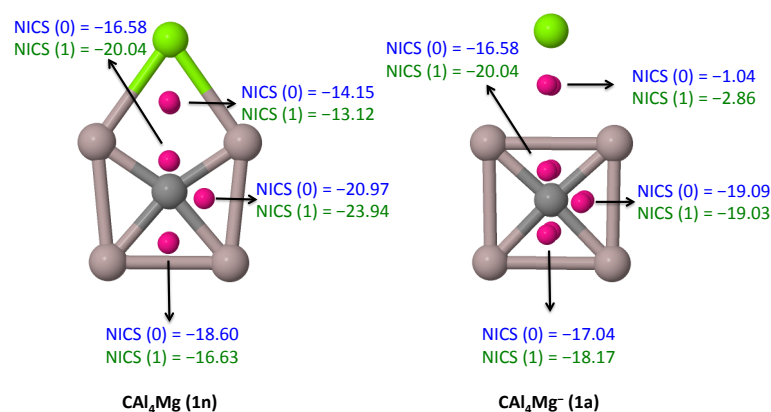


Figure 6. Nucleus independent chemical shifts (NICSs; in ppm) for CAI_4Mg (**1n**) and CAI_4Mg^- (**1a**) calculated at the $(U)\omega B97XD/6-311++G(2d,2p)$ level. NICS(1) (green color) is calculated at 1 Å above the ring, whereas NICS(0) (blue color) refers to on the plane values.

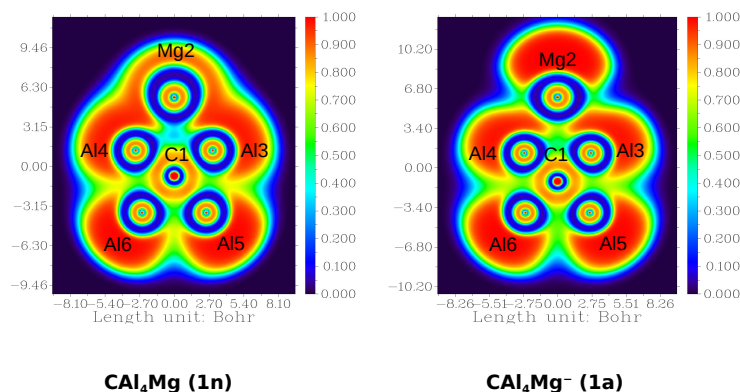


Figure 7. Color filled map of ELF for CAI_4Mg (**1n**) and CAI_4Mg^- (**1a**) calculated at the $(U)\omega B97XD/6-311++G(2d,2p)$ level. Relative geometric distances are shown in the abscissal and longitudinal coordinates. For clarity, the atomic label and index are added nearby the position of the corresponding atom.

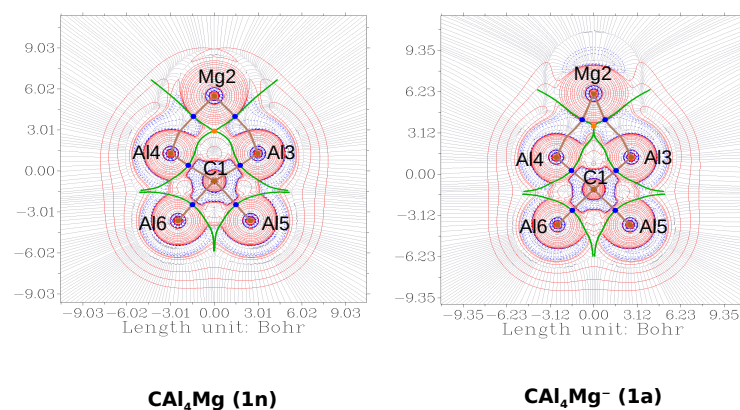


Figure 8. Contour map of the Laplacian of Electron Density ($\nabla^2\rho(r)$) with the bond paths for CAI_4Mg (**1n**) and CAI_4Mg^- (**1a**) calculated at the $(U)\omega B97XD/6-311++G(2d,2p)$ level. The blue lines show areas of charge concentration $\nabla^2\rho(r) \leq 0$, whereas the red lines show areas of charge depletion $\nabla^2\rho(r) \geq 0$. The brown dots represent the nucleus critical point or NCP. The brown lines connect NCP and bond critical points (BCP). The green line connecting RCP (ring critical point, orange dot) shows the inter-basin path. For clarity, the atomic label and index are added nearby the position of the corresponding atom.

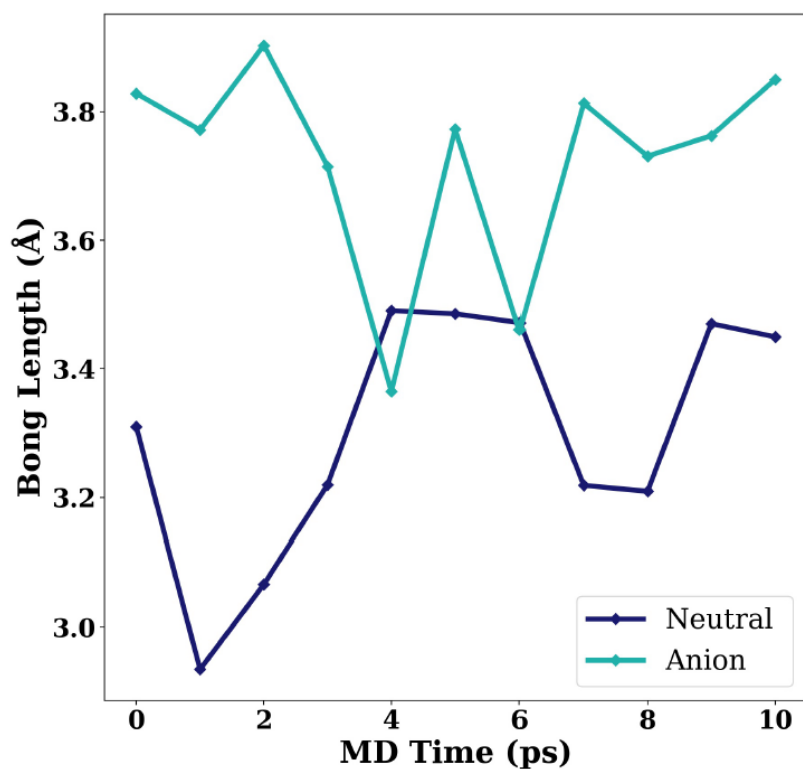


Figure 9. Bond length (C-Mg) evolution of CAI_4Mg (**1n**) and CAI_4Mg^- (**1a**) at 298 K in 10 ps ab initio MD simulations calculated at the $(\text{U})\omega\text{B97XD}/6\text{-311++G}(2\text{d},2\text{p})$ level.

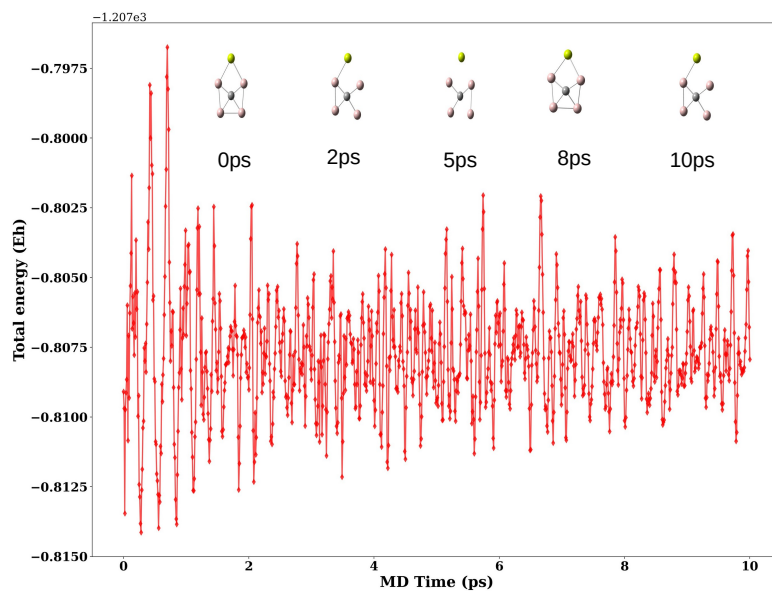


Figure 10. Energy evolution of CAI_4Mg (**1n**) at 298 K in 10 ps ab initio MD simulations calculated at the $\omega\text{B97XD}/6\text{-311++G}(2\text{d},2\text{p})$ level.

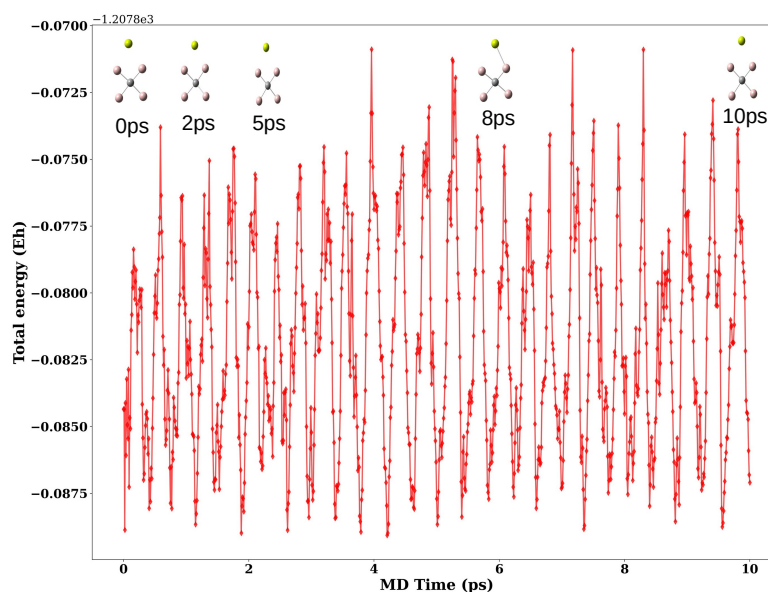


Figure 11. Energy evolution of $\text{CA}_{14}\text{Mg}^-$ (**1a**) at 298 K in 10 ps ab initio MD simulations calculated at the $U\omega\text{B97XD}/6\text{-}311++\text{G}(2\text{d},2\text{p})$ level.

3.1. Thermal Stability

Isomers with a ptC atom (**1n** and **1a**) turned out to be global minima after our extensive search on the neutral and anion PESs. The second most stable isomer (**2n**) for the neutral contains a tetrahedral tetracoordinate carbon, which is $2.63 \text{ kcal mol}^{-1}$ above **1n**. At CBS-QB3 level, this gap increases to $6.18 \text{ kcal mol}^{-1}$. In the case of anion, isomer **2a** lies 10.13 and $9.37 \text{ kcal mol}^{-1}$, respectively, above **1a** at $U\omega\text{B97XD}/6\text{-}311++\text{G}(2\text{d},2\text{p})$ and CBS-QB3 levels. This indirectly implies that the formation of **1a** is more favorable as there is no other isomer is close by within $\sim 10 \text{ kcal mol}^{-1}$. The bonding scenario for the carbon atom in **2a** is nearly tetrahedral. The adiabatic electron affinity of **1n** is 2.05 and 1.96 eV at the $(U)\omega\text{B97XD}/6\text{-}311++\text{G}(2\text{d},2\text{p})$ and CBS-QB3 levels, respectively. Therefore, detecting these systems are experimentally feasible.

3.2. Natural Atomic Charge and Wiberg Bond Indices

The atomic charge on the C atom is above $-2.70 |e|$ in both cases. The charge on all Al atoms are positive (0.41 and $0.56 |e|$ in **1n** and 0.17 and $0.44 |e|$ in **1a**). This results in a simultaneous operation of π -accepting and σ -donating effects stabilizing the ptC. As far as electronic structure is concerned, unlike the CA_{14}Be case [30], where ppC atom was established, here, due to increased ionic radii down the group (Be to Mg), the most stable structures exhibit ptC atom. Compared with the experimentally known molecule, CA_{14}H [7], where the H-atom binds with the bridge of the Al-Al bond, here Mg-atom binds on the opposite end where there is a dative Al-Al bond. The Wiberg bond index (WBI) [68] for this dative Al-Al bond is 0.37 and the WBI for C-Mg is negligibly small (0.06). Furthermore, the number of valence electrons in CA_{14}H is 17, and here it is perfectly 18 following the closed-shell valence electron rule suggested elsewhere [4]. Moreover, unlike CA_{14}H^- case, where the H-atom is still connected to the bridge of the Al-Al bond, here, the Mg atom in $\text{CA}_{14}\text{Mg}^-$ binds with the Al-Al bridge through ionic/covalent interactions at the center. WBI for Al-Mg and C-Mg in **1a** are 0.21 and 0.02, respectively. The C-Mg distances for neutral and anion are 3.31 and 3.83 Å, respectively. While the neutral molecule broke the valence electron rule in CA_{14}H , here, it is the anion, $\text{CA}_{14}\text{Mg}^-$, that breaks the rule with 19 valence electrons.

3.3. Bonding and Aromaticity

The Canonical molecular orbitals (CMOs) of the global minimum geometries of CAI_4Mg and CAI_4Mg^- are shown in Figure 4. Both the structures containing the ptC atom can be explained using these MOs. In particular, HOMO-4 (CAI_4Mg) exhibits π -delocalization, whereas HOMO, HOMO-2 and HOMO-5 shown there depict σ -delocalization. Likewise, for CAI_4Mg^- , π -delocalization can be seen in HOMO-5, whereas HOMO, HOMO-1 and HOMO-6 show σ -delocalization. While the Mg atom is directly bonded to the Al atoms in the neutral, it is bound to the Al atoms via ionic/covalent interactions in the anion. HOMO-6 (σ) clearly shows that there is an overlap between the Mg and Al atoms while other σ orbitals in the anion do not show an overlap, which justifies the mixed bonding character.

The overall bonding pattern in **1n** and **1a** can also be explained from AdNDP analysis, which covers not only Lewis bonding elements but also delocalized multi-center-2e bonds. For brevity, we show only the latter in Figure 5 to account for the $2\pi/6\sigma$ double aromaticity of the ptC in both the systems. Figure 5a,b,d reveals 3c-2e, 4c-2e and 5c-2e σ bonds with occupation numbers (ON) of 1.99, 2.00 and 2.00 $|e|$, respectively. Figure 5c indicates the 5c-2e π bond with ON of 2.00 $|e|$. Likewise, for the anion too, AdNDP orbitals (Figure 5, bottom row) depict the multi-center 2e bonds, which specifies the $2\pi/6\sigma$ double aromaticity of the ptC atom. In both the global minima, the π/σ -dual aromaticity can also be independently confirmed through NICS values. The latter computed at 0 (on the ring) and 1 Å (above the ring) for **1n** and **1a** are shown in Figure 6. All the values obtained for each triangle are negative in both cases. This implies that both σ - (NICS(0)) and π -aromaticity (NICS(1)) are operatives in these two global minimum geometries containing ptC atom.

3.4. Topological Analysis

Two color filled map of ELF for CAI_4Mg (**1n**) and CAI_4Mg^- (**1a**) is given in Figure 7. The ELF plot shows the delocalization of electron density within the molecule. The analysis further confirms that the interaction between the central C atom and four Al atoms is strong and the interaction between C and Mg atoms are much weaker. While the delocalization of electron density between Als and Mg are stronger, the delocalization between C and Mg are weaker in the neutral **1n** compared to anionic **1a**. This indicates that the addition of negative charge increases the interaction between the center (C atom) of the ptC system and the distant Mg atom.

We further analyzed the topology of electron density ($\rho(r)$) for the ptC geometries based on the Quantum Theory of Atoms In Molecules (QTAIM) [73]. The contour plots of the Laplacian of electron density ($\nabla^2\rho(r)$) along with bond paths and critical points for **1n** and **1a** are given in Figure 8. The topological parameters such as Lagrangian kinetic energy $G(r_c)$, potential energy density $V(r_c)$, energy density $E(r_c)$ or $H(r_c)$, $-G(r_c)/V(r_c)$ and $G(r_c)/\rho(r_c)$ at the critical points are given in Table 1. The bond paths indicate the bond between the central C atom with the four Al atoms. The electron density is found to be more between central C and Mg in the anionic **1a**. The low $\rho(r_c)$ values and positive $\nabla^2\rho(r_c)$ values suggest there is a closed-shell type of bonding involvement [74]. All the $H(r_c)$ with < 0 values confirm a partial covalent interaction [75–77]. There is no indication for noncovalent interaction as the ratio $-G(r_c)/V(r_c)$ lies in between 0.5 and 1 [78]. Some of the $G(r_c)/\rho(r_c)$ values (< 1) indicate bonding with partial covalent character.

Table 1. Electron density descriptors (in a.u.) at the (3, −1) bond critical points (BCP) and ring critical point (RCP, C1-Mg2) obtained from the (U)ωB97XD/6-311++G(2d,2p) level for CAI_4Mg (**1n**) and CAI_4Mg^- (**1a**). The topological parameters such as Lagrangian kinetic energy $G(r_c)$, potential energy density $V(r_c)$, energy density $E(r_c)$ or $H(r_c)$, $-G(r_c)/V(r_c)$ and $G(r_c)/\rho(r_c)$ at the critical points are also given.

Systems	BCP & RCP	$\rho(r_c)$	$\delta^2\rho(r_c)$	$G(r_c)$	$V(r_c)$	$H(r_c)$	ELF	$-G(r_c)/V(r_c)$	$G(r_c)/\rho(r_c)$
CAI_4Mg	Al4-Mg2	0.0263	0.0029	0.0076	−0.0144	−0.0068	0.4370	0.5260	0.2880
	C1-Al4	0.0832	0.3100	0.1050	−0.1330	−0.0277	0.1570	0.7890	1.2620
	Al6-C1	0.0672	0.2240	0.0766	−0.0972	−0.0206	0.1480	0.7880	1.1390
	C1-Mg2	0.0199	0.0104	0.0057	−0.0088	−0.0031	0.3500	0.6470	0.2870
	Al3-Mg2	0.0263	0.0029	0.0076	−0.0144	−0.0068	0.4370	0.5260	0.2870
	C1-Al3	0.0832	0.3100	0.1050	−0.1330	−0.0277	0.1570	0.7890	1.2620
	Al5-C1	0.0672	0.2240	0.0766	−0.0972	−0.0206	0.1480	0.7880	1.1390
CAI_4Mg^-	Al4-Mg2	0.0235	0.0056	0.0069	−0.0124	−0.0055	0.3920	0.5560	0.2930
	C1-Al4	0.0808	0.3160	0.1040	−0.1300	−0.0254	0.1470	0.8000	1.2870
	C1-Mg2	0.0227	−0.0034	0.0039	−0.0088	−0.0048	0.6370	0.4510	0.1740
	Al6-C1	0.0723	0.2650	0.0880	−0.1100	−0.0218	0.1440	0.8000	1.2170
	Al3-Mg2	0.0235	0.0056	0.0069	−0.0124	−0.0055	0.3920	0.5560	0.2940
	C1-Al3	0.0808	0.3160	0.1040	−0.1300	−0.0254	0.1470	0.8000	1.2870
	Al5-C1	0.0723	0.2650	0.0880	−0.1100	−0.0218	0.1440	0.8000	1.2170

3.5. Kinetic Stability

We carried out ab initio MD simulations using ADMP approach to evaluate the kinetic stability of **1n** and **1a**. We analyzed the changes in the structure and bond length between C and Mg, as well as changes in the energy. The time evolution of the bond length of **1n** and **1a** is shown in Figure 9. We checked the snapshots during the simulation from 0 to 10 ps at 298 K at intervals of 1 ps. The characteristic bond length (C-Mg) changes from 2.93 to 3.49 Å for neutral CAI_4Mg . For anionic CAI_4Mg^- , the range of fluctuation in bond length is 3.46–3.85 Å. In Figures 10 and 11, the evolution of energy (in a.u.) is shown up to 10 ps of simulation time at temperature 298 K for CAI_4Mg (**1n**) and CAI_4Mg^- (**1a**). A few geometries at different snapshots are given to show the structural changes during the simulation. The changes in energy (in a.u.) with time (in ps) shows the oscillation in energy for both cases (**1n** and **1a**). The range of oscillation of energy is comparatively higher for an anionic system (**1a**). The steady fluctuations in energy and consistency in the geometry suggest the kinetic stability of these molecules. For anion, the range is higher, which may be attributed to the extra negative charge present within the system. However, we note that the EA value obtained for the neutral is in the range of 1.96–2.05 eV.

4. Conclusions

Molecules with a ptC atom have been theoretically characterized for the first time in both CAI_4Mg (**1n**) and CAI_4Mg^- (**1a**). Their electronic structures reveal that the Mg atom makes a bond with Al atoms at a non-bridging position in the neutral, whereas it is bound to the Al atoms with a mixture of ionic/covalent interactions in the anion. The neutral molecule obeys the 18 valence electron rule but the anion breaks the rule with 19 valence electrons in total. However, both are stabilized by π/σ double aromaticity. More than the valence electron, it is the double aromaticity factor that governs the stabilization of these molecules. Topological analysis through ELF and the electron density plot confirm that both the systems contain a ptC atom. Ab initio MD simulations carried out at 298 K for 10 ps revealed that these molecules are kinetically stable. Considering the electron affinity values of 1.96–2.05 eV for the neutral, it is believed that the rule-breaking anion and then the rule-abiding neutral could be identified in the laboratory.

Supplementary Materials: The following are available online at <https://www.mdpi.com/2218-2004/9/2/24/s1>. Optimized geometries of high-energy isomers, Cartesian coordinates of all isomers, total energies, zero-point vibrational energies (ZPVEs), net dipole moment and relative energies without and with ZPVE corrections are given.

Author Contributions: Conceptualization, V.S.T.; methodology, A.A., V.S.T.; software, N.J., M.K., A.A., S.S.R.C., K.T., V.C. and V.S.T.; validation, V.S.T. and A.A.; formal analysis, N.J., M.K., V.S.T., A.A. and K.T.; investigation, V.S.T., K.T. and V.C.; resources, K.T., A.A. and V.S.T.; data curation, S.S.R.C. and V.S.T.; writing—original draft preparation, M.K. and V.S.T.; writing—review and editing, V.S.T. and A.A.; visualization, N.J., M.K., K.T., A.A. and V.S.T.; supervision, V.S.T. and A.A.; and project administration, V.S.T. All authors have read and agreed to the published version of the manuscript.

Funding: This research received no external funding. Computational support provided at the SDSU by DURIP Grant W911NF-10-1-0157 from the U.S. Department of Defense and by NSF CRIF Grant CHE-0947087 is gratefully acknowledged. Additional computational support provided at VIT, Vellore, India, through a research grant (Project. No. YSS/2014/001019) from the Science and Engineering Research Board, Department of Science and Technology, New Delhi, Government of India, is gratefully acknowledged.

Institutional Review Board Statement: Not applicable.

Informed Consent Statement: Not applicable.

Data Availability Statement: Data available in article or Supplementary Materials.

Acknowledgments: We acknowledge the resources of the Supercomputing facility at the Indian Institute of Technology Kharagpur established under National Supercomputing Mission (NSM), Government of India and supported by Centre for Development of Advanced Computing (CDAC), Pune. VST thanks Andrew L. Cooksy (SDSU, San Diego) for providing access to the computational resources. We also thank Raviprasad Aduri (BITS Pilani, Goa Campus) for his interest in this work.

Conflicts of Interest: The authors declare no conflict of interest.

Abbreviations

The following abbreviations are used in this manuscript:

ADMP	Atom-centered Density Matrix Propagation
AdNDP	Adaptive Natural Density Partitioning
CMOs	Canonical Molecular Orbitals
DFT	Density Functional Theory
ELF	Electron Localization Function
MD	Molecular Dynamics
NBO	Natural Bond Order
NICS	Nucleus Independent Chemical Shift
ptC	Planar Tetracoordinate Carbon
phC	Planar Hypercoordinate Carbon
ppC	Planar Pentacoordinate Carbon
WBI	Wiberg Bond Index

References

1. Erker, G. Planar-Tetracoordinate Carbon: Making Stable Anti-van't Hoff/Le Bel Compounds. *Comment. Inorg. Chem.* **1992**, *13*, 111–131. [[CrossRef](#)]
2. Röttger, D.; Erker, G. Compounds Containing Planar-Tetracoordinate Carbon. *Angew. Chem. Int. Ed. Engl.* **1997**, *36*, 812–827. [[CrossRef](#)]
3. Cotton, F.A.; Millar, M. The Probable Existence of A Triple Bond Between Two Vanadium Atoms. *J. Am. Chem. Soc.* **1977**, *99*, 7886. [[CrossRef](#)]
4. Boldyrev, A.I.; Simons, J. Tetracoordinated Planar Carbon in Pentaatomic Molecules. *J. Am. Chem. Soc.* **1998**, *120*, 7967–7972. [[CrossRef](#)]
5. Li, X.; Wang, L.S.; Boldyrev, A.I.; Simons, J. Tetracoordinated Planar Carbon in the Al_4C^- Anion. A Combined Photoelectron Spectroscopy and ab Initio Study. *J. Am. Chem. Soc.* **1999**, *121*, 6033–6038. [[CrossRef](#)]

6. Keese, R. Carbon Flatland: Planar Tetracoordinate Carbon and Fenestranes. *Chem. Rev.* **2006**, *106*, 4787–4808. [[CrossRef](#)] [[PubMed](#)]
7. Xu, J.; Zhang, X.; Yu, S.; Ding, Y.H.; Bowen, K.H. Identifying the Hydrogenated Planar Tetracoordinate Carbon: A Combined Experimental and Theoretical Study of CA_4H and CA_4H^- . *J. Phys. Chem. Lett.* **2017**, *8*, 2263–2267. [[CrossRef](#)]
8. Ebner, F.; Greb, L. Calix[4]pyrrole Hydridosilicate: The Elusive Planar Tetracoordinate Silicon Imparts Striking Stability to Its Anionic Silicon Hydride. *J. Am. Chem. Soc.* **2018**, *140*, 17409–17412. [[CrossRef](#)]
9. Li, X.; Zhang, H.F.; Wang, L.S.; Geske, G.; Boldyrev, A. Pentaatomic Tetracoordinate Planar Carbon, $[CA_4]^{2-}$: A New Structural Unit and Its Salt Complexes. *Angew. Chem. Int. Ed.* **2000**, *39*, 3630–3632. [[CrossRef](#)]
10. Ghana, P.; Rump, J.; Schnakenburg, G.; Arz, M.I.; Filippou, A.C. Planar Tetracoordinated Silicon (ptSi): Room-Temperature Stable Compounds Containing Anti-van't Hoff/Le Bel Silicon. *J. Am. Chem. Soc.* **2020**, *143*, 420–432. [[CrossRef](#)]
11. Hoffmann, R.; Alder, R.W.; Wilcox, C.F. Planar Tetracoordinate Carbon. *J. Am. Chem. Soc.* **1970**, *92*, 4992–4993. [[CrossRef](#)]
12. Collins, J.B.; Dill, J.D.; Jemmis, E.D.; Apeloig, Y.; Schleyer, P.V.R.; Seeger, R.; Pople, J.A. Stabilization of Planar Tetracoordinate Carbon. *J. Am. Chem. Soc.* **1976**, *98*, 5419–5427. [[CrossRef](#)]
13. Merino, G.; Méndez-Rojas, M.A.; Beltrán, H.I.; Corminboeuf, C.; Heine, T.; Vela, A. Theoretical Analysis of the Smallest Carbon Cluster Containing a Planar Tetracoordinate Carbon. *J. Am. Chem. Soc.* **2004**, *126*, 16160–16169. [[CrossRef](#)]
14. Suresh, C.H.; Frenking, G. Direct 1-3 Metal-Carbon Bonding and Planar Tetracoordinated Carbon in Group 6 Metallocyclobutadienes. *Organometallics* **2010**, *29*, 4766–4769. [[CrossRef](#)]
15. Thirumoorthy, K.; Karton, A.; Thimmakondur, V.S. From High-Energy C_7H_2 Isomers with A Planar Tetracoordinate Carbon Atom to An Experimentally Known Carbene. *J. Phys. Chem. A* **2018**, *122*, 9054–9064. [[CrossRef](#)]
16. Raghunathan, S.; Yadav, K.; Rojisha, V.C.; Jaganade, T.; Prathyusha, V.; Bikkina, S.; Lourderaj, U.; Priyakumar, U.D. Transition Between [R]- and [S]-Stereoisomers without Bond Breaking. *Phys. Chem. Chem. Phys.* **2020**, *22*, 14983–14991. [[CrossRef](#)]
17. Yang, L.M.; Ganz, E.; Chen, Z.; Wang, Z.X.; Schleyer, P.V.R. Four Decades of the Chemistry of Planar Hypercoordinate Compounds. *Angew. Chem. Int. Ed.* **2015**, *54*, 9468–9501. [[CrossRef](#)]
18. Yañez, O.; Vásquez-Espinal, A.; Báez-Grez, R.; Rabanal-León, W.A.; Osorio, E.; Ruiz, L.; Tiznado, W. Carbon Rings Decorated with Group 14 Elements: New Aromatic Clusters Containing Planar Tetracoordinate Carbon. *New J. Chem.* **2019**, *43*, 6781–6785.
19. Thirumoorthy, K.; Thimmakondur, V.S. Flat Crown Ethers with Planar Tetracoordinate Carbon Atoms. *Int. J. Quantum Chem.* **2021**, *121*, e26479. [[CrossRef](#)]
20. van't Hoff, J.H. A Suggestion Looking to the Extension into Space of the Structural Formulas at Present Used in Chemistry. And a Note Upon the Relation between the Optical Activity and the Chemical Constitution of Organic Compounds. *Arch. Neerl. Sci. Exactes Nat.* **1874**, *9*, 445–454.
21. Le-Bel, J.A. On the Relations Which Exist Between the Atomic Formulas of Organic Compounds and the Rotatory Power of Their Solutions. *Bull. Soc. Chim. Fr.* **1874**, *22*, 337–347.
22. Monkhurst, H.J. Activation Energy for Interconversion of Enantiomers Containing an Asymmetric Carbon Atom without Breaking Bonds. *Chem. Commun. (Lond.)* **1968**, 1111–1112. [[CrossRef](#)]
23. Sateesh, B.; Srinivas Reddy, A.; Narahari Sastry, G. Towards Design of the Smallest Planar Tetracoordinate Carbon and Boron Systems. *J. Comput. Chem.* **2007**, *28*, 335–343. [[CrossRef](#)] [[PubMed](#)]
24. Cui, Z.H.; Contreras, M.; Ding, Y.H.; Merino, G. Planar Tetracoordinate Carbon versus Planar Tetracoordinate Boron: The Case of CB_4 and Its Cation. *J. Am. Chem. Soc.* **2011**, *133*, 13228–13231. [[CrossRef](#)] [[PubMed](#)]
25. Cui, Z.H.; Ding, Y.H.; Cabellos, J.L.; Osorio, E.; Islas, R.; Restrepo, A.; Merino, G. Planar tetracoordinate carbons with a double bond in CA_3E clusters. *Phys. Chem. Chem. Phys.* **2015**, *17*, 8769–8775. [[CrossRef](#)] [[PubMed](#)]
26. Nandula, A.; Trinh, Q.T.; Saeys, M.; Alexandrova, A.N. Origin of Extraordinary Stability of Square-Planar Carbon Atoms in Surface Carbides of Cobalt and Nickel. *Angew. Chem. Int. Ed.* **2015**, *54*, 5312–5316. [[CrossRef](#)]
27. Thimmakondur, V.S.; Thirumoorthy, K. $Si_3C_2H_2$ Isomers with A Planar Tetracoordinate Carbon or Silicon Atom(s). *Comput. Theor. Chem.* **2019**, *1157*, 40–46. [[CrossRef](#)]
28. Guo, J.C.; Feng, L.Y.; Dong, C.; Zhai, H.J. Ternary 12-electron $CBe_3X_3^+$ ($X = H, Li, Na, Cu, Ag$) Clusters: Planar Tetracoordinate Carbons and Superalkali Cations. *Phys. Chem. Chem. Phys.* **2019**, *21*, 22048–22056. [[CrossRef](#)] [[PubMed](#)]
29. Thirumoorthy, K.; Cooksy, A.; Thimmakondur, V.S. $Si_2C_5H_2$ Isomers—Search Algorithms Versus Chemical Intuition. *Phys. Chem. Chem. Phys.* **2020**, *22*, 5865–5872. [[CrossRef](#)]
30. Jimenez-Halla, J.O.C.; Wu, Y.B.; Wang, Z.X.; Islas, R.; Heine, T.; Merino, G. CA_4Be and $CA_3Be_2^-$: Global Minima with A Planar Pentacoordinate Carbon Atom. *Chem. Commun.* **2010**, *46*, 8776–8778. [[CrossRef](#)] [[PubMed](#)]
31. Thimmakondur, V.S.; Thirumoorthy, K. Flat Crown Ethers with Planar Tetracoordinate Carbon Atoms. *ChemRxiv* **2020**. [[CrossRef](#)]
32. Job, N.; Karton, A.; Thirumoorthy, K.; Cooksy, A.L.; Thimmakondur, V.S. Theoretical Studies of SiC_4H_2 Isomers Delineate Three Low-Lying Silylidenes Are Missing in the Laboratory. *J. Phys. Chem. A* **2020**, *124*, 987–1002. [[CrossRef](#)] [[PubMed](#)]
33. Pei, Y.; An, W.; Ito, K.; Schleyer, P.V.R.; Zeng, X.C. Planar Pentacoordinate Carbon in CA_5^+ : A Global Minimum. *J. Am. Chem. Soc.* **2008**, *130*, 10394–10400. [[CrossRef](#)] [[PubMed](#)]
34. Guo, J.C.; Feng, L.Y.; Zhang, X.Y.; Zhai, H.J. Star-Like $CBe_5Au_5^+$ Cluster: Planar Pentacoordinate Carbon, Superalkali Cation, and Multifold (π and σ) Aromaticity. *J. Phys. Chem. A* **2018**, *122*, 1138–1145. [[CrossRef](#)]
35. Vassilev-Galindo, V.; Pan, S.; Donald, J.K.; Merino, G. Planar Pentacoordinate Carbons. *Nat. Chem. Rev.* **2018**, *2*, 0114. [[CrossRef](#)]
36. Exner, K.; Schleyer, P.V.R. Planar Hexacoordinate Carbon: A Viable Possibility. *Science* **2000**, *290*, 1937–1940. [[CrossRef](#)] [[PubMed](#)]

37. Averkiev, B.B.; Zubarev, D.Y.; Wang, L.M.; Huang, W.; Wang, L.S.; Boldyrev, A.I. Carbon Avoids Hypercoordination in CB_6^- , CB_6^{2-} , and $C_2B_5^-$ Planar Carbon-Boron Clusters. *J. Am. Chem. Soc.* **2008**, *130*, 9248–9250. [[CrossRef](#)] [[PubMed](#)]
38. Ito, K.; Chen, Z.; Corminboeuf, C.; Wannere, C.S.; Zhang, X.H.; Li, Q.S.; Schleyer, P.V.R. Myriad Planar Hexacoordinate Carbon Molecules Inviting Synthesis. *J. Am. Chem. Soc.* **2007**, *129*, 1510–1511. [[CrossRef](#)] [[PubMed](#)]
39. Wu, Y.B.; Duan, Y.; Lu, G.; Lu, H.G.; Yang, P.; Schleyer, P.V.R.; Merino, G.; Islas, R.; Wang, Z.X. D_{3h} $CN_3Be_3^+$ and $CO_3Li_3^+$: Viable Planar Hexacoordinate Carbon Prototypes. *Phys. Chem. Chem. Phys.* **2012**, *14*, 14760–14763. [[CrossRef](#)]
40. Zhang, C.F.; Han, S.J.; Wu, Y.B.; Lu, H.G.; Lu, G. Thermodynamic Stability versus Kinetic Stability: Is the Planar Hexacoordinate Carbon Species D_{3h} $CN_3Mg_3^+$ Viable? *J. Phys. Chem. A* **2014**, *118*, 3319–3325. [[CrossRef](#)] [[PubMed](#)]
41. Zhai, H.J.; Alexandrova, A.N.; Birch, K.A.; Boldyrev, A.I.; Wang, L.S. Hepta- and Octacoordinate Boron in Molecular Wheels of Eight- and Nine-Atom Boron Clusters: Observation and Confirmation. *Angew. Chem. Int. Ed.* **2003**, *42*, 6004–6008. [[CrossRef](#)] [[PubMed](#)]
42. Kalita, A.J.; Rohman, S.S.; Kashyap, C.; Ullah, S.S.; Guha, A.K. Double aromaticity in a $BBe_6H_6^+$ cluster with a planar hexacoordinate boron structure. *Chem. Commun.* **2020**, *56*, 12597–12599. [[CrossRef](#)]
43. Kalita, A.J.; Rohman, S.S.; Kashyap, C.; Ullah, S.S.; Baruah, I.; Guha, A.K. Planar Pentacoordinate Nitrogen in a Pseudo-Double-Aromatic $NBe_5H_4^+$ Cluster. *Inorg. Chem.* **2020**, *59*, 17880–17883. [[CrossRef](#)] [[PubMed](#)]
44. Wang, Y.; Li, F.; Li, Y.; Chen, Z. Semi-Metallic Be_5C_2 Monolayer Global Minimum with Quasi-Planar Pentacoordinate Carbons and Negative Poisson's Ratio. *Nat. Commun.* **2016**, *7*, 11488. [[CrossRef](#)] [[PubMed](#)]
45. Li, Y.; Liao, Y.; Chen, Z. Be_2C Monolayer with Quasi-Planar Hexacoordinate Carbons: A Global Minimum Structure. *Angew. Chem. Int. Ed.* **2014**, *53*, 7248–7252. [[CrossRef](#)] [[PubMed](#)]
46. Guo, J.C.; Feng, L.Y.; Dong, C.; Zhai, H.J. Planar Pentacoordinate versus Tetracoordinate Carbons in Ternary CBe_4Li_4 and $CBe_4Li_4^{2-}$ Clusters. *J. Phys. Chem. A* **2018**, *122*, 8370–8376. [[CrossRef](#)]
47. Thirumoorthy, K.; Chandrasekaran, V.; Cooksy, A.L.; Thimmakondur, V.S. Kinetic Stability of $Si_2C_5H_2$ Isomer with a Planar Tetracoordinate Carbon Atom. *Chemistry* **2021**, *3*, 13–27. [[CrossRef](#)]
48. Wang, Z.X.; Zhang, C.G.; Chen, Z.F.; Schleyer, P.V.R. Planar Tetracoordinate Carbon Species Involving Beryllium Substituents. *Inorg. Chem.* **2008**, *47*, 1332. [[CrossRef](#)]
49. Buchner, M.R. Beryllium Coordination Chemistry and Its Implications on the Understanding of Metal Induced Immune Responses. *Chem. Commun.* **2020**, *56*, 8895–8907. [[CrossRef](#)]
50. Naglav, D.; Buchner, M.R.; Bendt, G.; Kraus, F.; Schulz, S. Off the Beaten Track—A Hitchhiker's Guide to Beryllium Chemistry. *Angew. Chem. Int. Ed.* **2016**, *55*, 10562–10576. [[CrossRef](#)]
51. Nandi, S.; McAnanama-Brereton, S.R.; Waller, M.P.; Anoop, A. A Tabu-Search Based Strategy for Modeling Molecular Aggregates and Binary Reactions. *Comput. Theor. Chem.* **2017**, *1111*, 69–81. [[CrossRef](#)]
52. Khatun, M.; Majumdar, R.S.; Anoop, A. A Global Optimizer for Nanoclusters. *Front. Chem.* **2019**, *7*, 644. [[CrossRef](#)] [[PubMed](#)]
53. Neese, F. Software Update: The ORCA Program System, Version 4.0. *Wiley Interdiscip. Rev. Comput. Mol. Sci.* **2018**, *8*, e1327. [[CrossRef](#)]
54. Perdew, J.P.; Burke, K.; Wang, Y. Generalized Gradient Approximation for the Exchange-Correlation Hole of a Many-Electron System. *Phys. Rev. B* **1996**, *54*, 16533. [[CrossRef](#)] [[PubMed](#)]
55. Weigend, F.; Ahlrichs, R. Balanced Basis Sets of Split Valence, Triple Zeta Valence and Quadruple Zeta Valence Quality for H to Rn: Design and Assessment of Accuracy. *Phys. Chem. Chem. Phys.* **2005**, *7*, 3297–3305. [[CrossRef](#)] [[PubMed](#)]
56. Grimme, S.; Antony, J.; Ehrlich, S.; Krieg, H. A Consistent and Accurate Ab Initio Parametrization of Density Functional Dispersion Correction (DFT-D) for the 94 Elements H-Pu. *J. Chem. Phys.* **2010**, *132*, 154104. [[CrossRef](#)] [[PubMed](#)]
57. Becke, A.D.; Johnson, E.R. Exchange-Hole Dipole Moment and the Dispersion Interaction. *J. Chem. Phys.* **2005**, *122*, 154104. [[CrossRef](#)] [[PubMed](#)]
58. Grimme, S.; Ehrlich, S.; Goerigk, L. Effect of the Damping Function in Dispersion Corrected Density Functional Theory. *J. Comput. Chem.* **2011**, *32*, 1456–1465. [[CrossRef](#)] [[PubMed](#)]
59. Chai, J.D.; Head-Gordon, M. Long-Range Corrected Hybrid Density Functionals with Damped Atom-Atom Dispersion Corrections. *Phys. Chem. Chem. Phys.* **2008**, *10*, 6615–6620. [[CrossRef](#)] [[PubMed](#)]
60. Krishnan, R.; Binkley, J.S.; Seeger, R.; Pople, J.A. Self-Consistent Molecular Orbital Methods. XX. A Basis Set for Correlated Wave Functions. *J. Chem. Phys.* **1980**, *72*, 650–654. [[CrossRef](#)]
61. Clark, T.; Chandrasekhar, J.; Spitznagel, G.W.; Schleyer, P.V.R. Efficient Diffuse Function-Augmented Basis Sets for Anion Calculations. III. The 3-21+G Basis Set for First-Row Elements, Li-F. *J. Comput. Chem.* **1983**, *4*, 294–301. [[CrossRef](#)]
62. Montgomery, J.A.; Frisch, M.J.; Ochterski, J.W.; Petersson, G.A. A Complete Basis Set Model Chemistry. VI. Use of Density Functional Geometries and Frequencies. *J. Chem. Phys.* **1999**, *110*, 2822–2827. [[CrossRef](#)]
63. Bauernschmitt, R.; Ahlrichs, R. Stability Analysis for Solutions of the Closed Shell Kohn-Sham Equation. *J. Chem. Phys.* **1996**, *104*, 9047–9052. [[CrossRef](#)]
64. Schleyer, P.V.R.; Maerker, C.; Dransfeld, A.; Jiao, H.; van Eikema Hommes, N.J.R. Nucleus-Independent Chemical Shifts: A Simple and Efficient Aromaticity Probe. *J. Am. Chem. Soc.* **1996**, *118*, 6317–6318. [[CrossRef](#)]
65. Zubarev, D.Y.; Boldyrev, A.I. Developing Paradigms of Chemical Bonding: Adaptive Natural Density Partitioning. *Phys. Chem. Chem. Phys.* **2008**, *10*, 5207–5217. [[CrossRef](#)] [[PubMed](#)]

66. Zubarev, D.Y.; Boldyrev, A.I. Revealing Intuitively Assessable Chemical Bonding Patterns in Organic Aromatic Molecules via Adaptive Natural Density Partitioning. *J. Org. Chem.* **2008**, *73*, 9251–9258. [[CrossRef](#)] [[PubMed](#)]
67. Reed, A.E.; Weinstock, R.B.; Weinhold, F. Natural Population Analysis. *J. Chem. Phys.* **1985**, *83*, 735–746. [[CrossRef](#)]
68. Glendening, E.D.; Weinhold, F. Natural Resonance Theory: I. General Formalism. *J. Comput. Chem.* **1998**, *19*, 593–609. [[CrossRef](#)]
69. Lee, T.J.; Taylor, P.R. A Diagnostic for Determining the Quality of Single-Reference Electron Correlation Methods. *Int. J. Quantum Chem.* **1989**, *36*, 199–207. [[CrossRef](#)]
70. Frisch, M.J.; Trucks, G.W.; Schlegel, H.B.; Scuseria, G.E.; Robb, M.A.; Cheeseman, J.R.; Scalmani, G.; Barone, V.; Petersson, G.A.; Nakatsuji, H.; et al. *Gaussian 16 Revision B.01*; Gaussian Inc.: Wallingford, CT, USA, 2016.
71. Lu, T.; Chen, F. Multiwfn: A Multifunctional Wavefunction Analyzer. *J. Comput. Chem.* **2012**, *33*, 580–592. [[CrossRef](#)] [[PubMed](#)]
72. Schlegel, H.B.; Millam, J.M.; Iyengar, S.S.; Voth, G.A.; Daniels, A.D.; Scuseria, G.E.; Frisch, M.J. Ab Initio Molecular Dynamics: Propagating the Density Matrix with Gaussian Orbitals. *J. Chem. Phys.* **2001**, *114*, 9758–9763. [[CrossRef](#)]
73. Bader, R.F.W. *Atoms in Molecules: A Quantum Theory*. 1990. Available online: <http://www.aim2000.de/> (accessed on 11 March 2021).
74. Cremer, D.; Kraka, E. Chemical Bonds without Bonding Electron Density—Does the Difference Electron-Density Analysis Suffice for a Description of the Chemical Bond? *Angew. Chem. Int. Ed. Engl.* **1984**, *23*, 627–628. [[CrossRef](#)]
75. Macchi, P.; Proserpio, D.M.; Sironi, A. Experimental Electron Density in a Transition Metal Dimer: Metal-Metal and Metal-Ligand Bonds. *J. Am. Chem. Soc.* **1998**, *120*, 13429–13435. [[CrossRef](#)]
76. Macchi, P.; Garlaschelli, L.; Martinengo, S.; Sironi, A. Charge Density in Transition Metal Clusters: Supported vs Unsupported Metal-Metal Interactions. *J. Am. Chem. Soc.* **1999**, *121*, 10428–10429. [[CrossRef](#)]
77. Novozhilova, I.V.; Volkov, A.V.; Coppens, P. Theoretical Analysis of the Triplet Excited State of the $[\text{Pt}_2(\text{H}_2\text{P}_2\text{O}_5)_4]^{4-}$ Ion and Comparison with Time-Resolved X-ray and Spectroscopic Results. *J. Am. Chem. Soc.* **2003**, *125*, 1079–1087. [[CrossRef](#)]
78. Ziólkowski, M.; Grabowski, S.J.; Leszczynski, J. Cooperativity in Hydrogen-Bonded Interactions: Ab Initio and “Atoms in Molecules” Analyses. *J. Phys. Chem. A* **2006**, *110*, 6514–6521. [[CrossRef](#)] [[PubMed](#)]